Supplementary Information

1. Characterization of AA-G Hybrids

The homogeneous aqueous solutions of AA-G hybrids have been shown as stable for more than three months with concentrations over 5 mg/mL (Figure S1). In contrast, the reduction of G oxide dispersion without AA as the stabilizer led to the precipitation of G after being stored for less than 2 weeks, implying the significant modification effect of AA. The UV-vis spectra of G oxide and AA-G are compared in Figure S2. The G oxide dispersion displays a maximum absorption at 231 nm which is due to the π-π^* transition of aromatic C=C bonds and a shoulder at ~290-300 nm which corresponds to the n-π^* transition of the C=O bonds.[1] Whereas, the absorption spectrum of AA-G presents increased absorption in the whole spectral region and a maximum absorption peak at 270 nm without a shoulder at ~290-300 nm, which are ascribed to the restored electronic conjugation within G.[2] The present result resembles the case of aqueous dispersion of G by lignin and cellulose derivatives,[1] which undoubtedly indicates the formation of AA-G hybrids from attaching AA on G. The morphology and component of AA-G hybrids were further characterized by transmission electron microscopy (TEM), atomic force microscopy (AFM), thermogravimetric analysis (TGA) and FT-IR. FT-IR spectra of AA and AA-G are shown in Figure S3. The gross resemblance in both spectral features and peak positions for several vibrational modes guarantees a successful attachment of AA onto G. For example, the strong band at 1150 cm^{-1} corresponds to the asymmetric glycosidic vibration ν_a(C-O-C); the bands at 1075 and 1017 cm^{-1} correspond to the coupled stretch vibration, ν(C-C/C-O); the broadband at 3337 cm^{-1} arises from the O-H vibrations; the narrowband at 2924 cm^{-1} correspond to amylose backbone absorptions, ν(C-H); and pyranose ring vibrations at the spectral region from 500-900 cm^{-1}.[1-3] The appearance of this IR band and those in the fingerprint regions indicate clearly that AAs cannot be removed from the solid materials (AA-G) by extensive washing with deionized water; thus, AA molecules have covered the surface of G. It is worth pointing out that the shifts at 1030, 1075, and 1017 cm^{-1} of the glycosidic deformation and ring stretch vibration in the spectra of AA and AA-G are indicative of a conformational change of the amylose chain of AA when it attached to G.[4] The amphiphilic properties of amylose have been clearly illustrated, wherein all the hydroxyls are disposed on one side of the chain backbone, making it hydrophilic, while the methines make up the other, relatively apolar, face of the ribbon.[6,7] In addition, noncovalent modification of SWNTs with amylose through methine-SWNTs hydrophobic interactions was also reported.[8,9] Hence, the formation of hydrophobic interactions between amylose chains and G is strongly supported, which is in accordance with the above experimental facts and FT-IR data.

TGA was used to estimate the amount of AA molecules on the surface of G in AA-G hybrids. Figure S4 displays the weight losses of AA, G, and AA-G. It is found that the weight loss at the low temperature region (about 300 °C) could be mainly attributed to the decomposition of AAs. Accordingly, the amount of AA molecules was determined to be 50 wt% (about one glucose unit per 13 carbon atoms), indicating that a number of AA molecules could be adsorbed on the surface of G.

The morphology of AA-G was observed by TEM and AFM. The AFM image (Figure S5A) of AA-G clearly shows the flake-like nanostructure. The corresponding cross-sectional view indicates that the average thickness of AA-G is *ca.* 3.6 nm, which is a typical characteristic of polymer-coated G nanosheets produced from the reduction of the exfoliated G oxide.[10-12] The greater thickness of AA-G than that of G oxide could be attributed to the AA molecules grafted onto both sides of G. TEM image (Figure S5B) also illustrates the well dispersed flake-like shapes of AA-G. The sizes of the flakes are in accordance with that observed by AFM. Particularly, little distortions caused by the extreme lack of thickness of the AA-G lead to a wrinkled topology.

2. Fluorescence resonance energy transfer (FRET)

Additional support for the idea that the fluorescence recovery of the G-based platform arose from formation of helical complex came from FRET experiments. 1-Pyrenemethylamine (PyMA, λ_{em}=400 nm) and Rhodamin 6G (R6G, λ_{abs}=500-530 nm) were selected as optical labels. Both PyMA and R6G could compose FRET pairs with anthracene (the end-labeled dye of AA, λ_{abs}=400 nm, λ_{em}=500 nm) by acting as the energy donor or acceptor, respectively. The FRET would be happened if PyMA (or R6G) form inclusion complexes with AA, because the inclusion association can decrease the distance between anthracene and PyMA (or R6G) to fulfill the basic requirement of a FRET process. Therefore, it is possible to monitor the formation of inclusion complexes by recording the fluorescence emission. Upon adding PyMA, excitation (λ_{ex}=317 nm) of the PyMA was accompanied by a FRET process, leading to the emission of the anthracene at 500 nm (Figure S8). However, a FRET process from anthracene to R6G was not observed in the presence of R6G (Figure S9A) and the fluorescence of R6G was completely quenched (Figure S9B). We attributed the results to the fact that the amylose chain of AA can only selectively associate to slender targets forming inclusion complexes with inner cavity size less than 0.78 nm.[13-15] Compared to the slender PyMA (≤0.78 nm), R6G (>0.78 nm) is bulky and hence cannot be included by AA to release it from G and achieve a FRET process. The results in turn indicated that formation of inclusion complex was responsible for the release of AA and the consequent fluorescence recovery.

References

1. Ang, P.K., et al., *High-Throughput Synthesis of Graphene by Intercalation−Exfoliation of Graphite Oxide and Study of Ionic Screening in Graphene Transistor.* Acs Nano, 2009. **3**(11): p. 3587-3594.

2. Li, D., et al., *Processable aqueous dispersions of graphene nanosheets.* Nat Nanotechnol, 2008. **3**(2): p. 101-105.

3. Yang, Q., et al., *Fabrication of High-Concentration and Stable Aqueous Suspensions of Graphene Nanosheets by Noncovalent Functionalization with Lignin and Cellulose Derivatives.* Journal of Physical Chemistry C, 2010. **114**(9): p. 3811-3816.

4. Yang, L. and L.-M. Zhang, *Chemical structural and chain conformational characterization of some bioactive polysaccharides isolated from natural sources.* Carbohydrate Polymers, 2009. **76**: p. 349–361.

5. Li, H. and C. Han, *Sonochemical Synthesis of Cyclodextrin-Coated Quantum Dots for Optical Detection of Pollutant Phenols in Water.* Chem. Mater., 2008. **20**: p. 6053–6059.

6. Balasubramanian, D., B. Raman, and C.S. Sundari, *Polysaccharides as Amphiphiles.* Journal of the American Chemical Society, 1993. **115**: p. 74-77.

7. Sivakama Sundari, C., B. Raman, and D. Balasubramanian, *Hydrophobic surfaces in oligosaccharides: linear dextrims are amphiphilic chains.* Biochimica et Biophysica Acta (BBA) - Biomembranes, 1991. **1065**(1): p. 35-41.

8. Star, A., et al., *Starched Carbon Nanotubes.* Angewandte Chemie International Edition, 2002. **41**(14): p. 2508-2512.

9. Kim, O.-K., et al., *Solubilization of Single-Wall Carbon Nanotubes by Supramolecular Encapsulation of Helical Amylose* Journal of the American Chemical Society, 2003. **125**(15): p. 4426-4427.

10. Patil, A.J., et al., *Aqueous Stabilization and Self-Assembly of Graphene Sheets into Layered Bio-Nanocomposites using DNA.* Advanced Materials, 2009. **21**(31): p. 3159-3164.

11. Bai, H., et al., *Non-covalent functionalization of graphene sheets by sulfonated polyaniline.* Chemical Communications, 2009(13): p. 1667-1669.

12. Stankovich, S., et al., *Stable aqueous dispersions of graphitic nanoplatelets via the reduction of exfoliated graphite oxide in the presence of poly(sodium 4-styrenesulfonate).* Journal of Materials Chemistry, 2006. **16**(2): p. 155-158.

13. Wei, W., B. Guo, and J.-M. Lin, *Helical- and ahelical-dependent chiral recognition mechanisms in capillary electrophoresis using amylose as the selector.* Electrophoresis, 2009. **30**: p. 1380-1387.

14. Tozuka, Y., et al., *Specific inclusion mode of guest compounds in the amylose complex analyzed by solid state NMR spectroscopy.* Chemical & Pharmaceutical Bulletin, 2006. **54**(8): p. 1097-1101.

15. Yamashita, Y.-h., J. Ryugo, and K. Monobe, *An Electron Microscopic Study on Crystals of Amylose V Complexes.* Journal of Electron Microscopy, 1973. **22**(1): p. 19-26.

Fig. S1. Photograph of 5 mg/mL anthracene-labeled amylose and graphene (AA-G) hybrids in water.

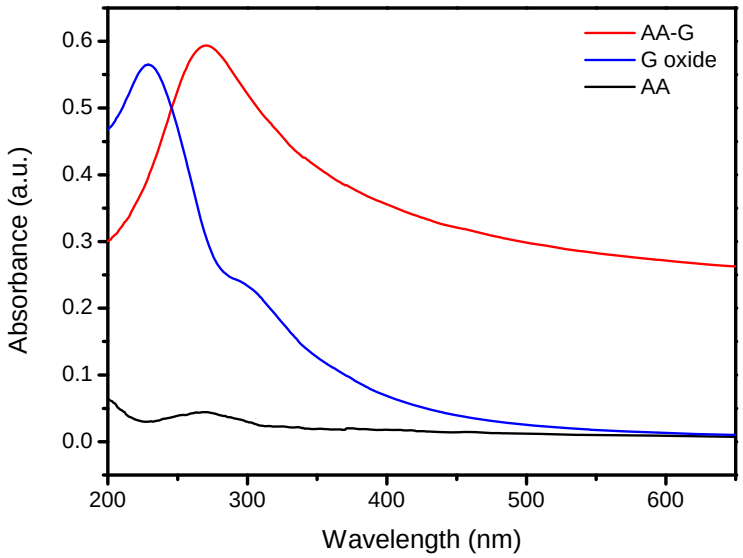

Fig. S2. UV-vis spectra of AA, G oxide and AA-G aqueous solutions.

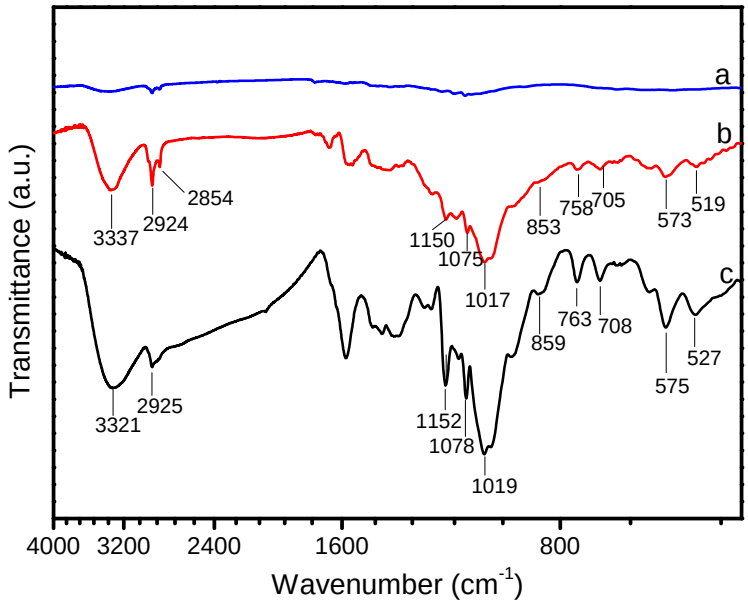

Fig. S3. FT-IR spectra of G (a), AA-G (b), and AA (c).

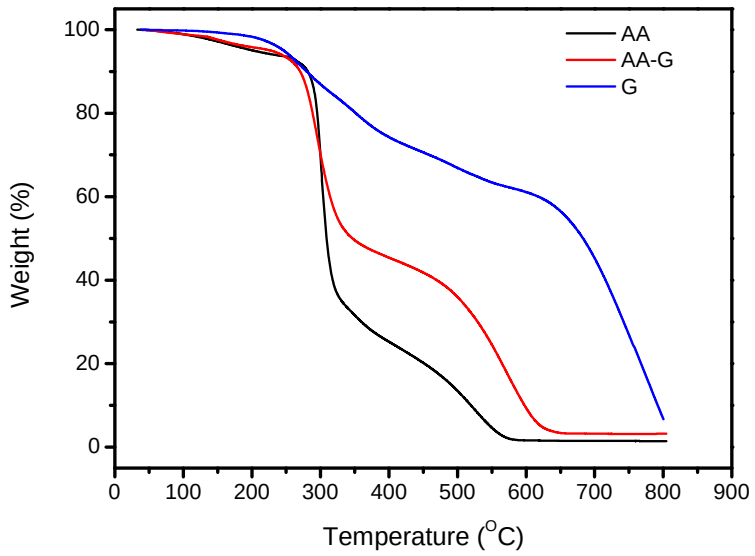

Fig. S4. TGA of AA, AA-G, and G.

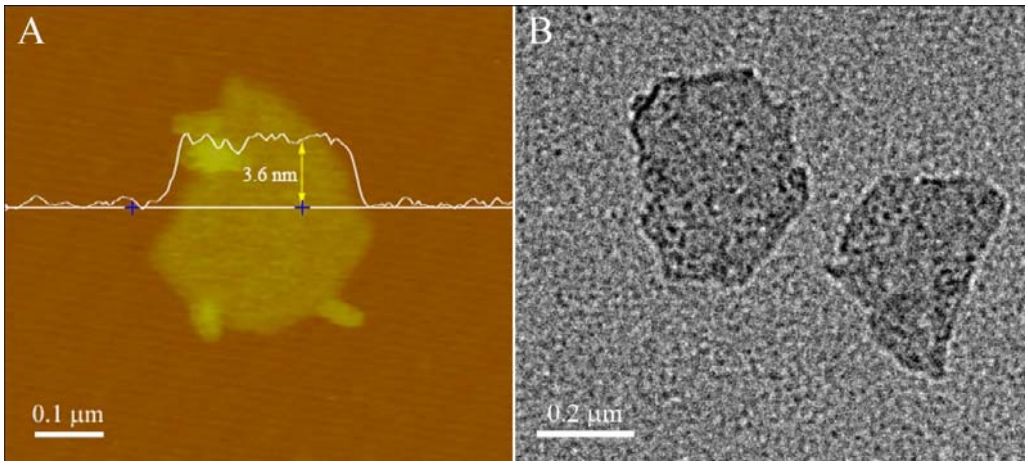

Fig. S5. AFM image (a) and TEM graph (b) of AA-G.

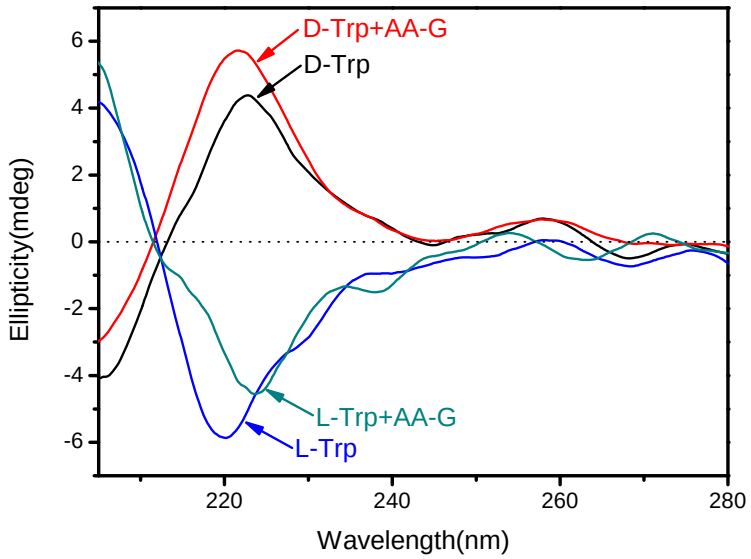

Fig. S6. CD spectra of 100 μM D-, L-Trp in the absence and presence of 0.1 wt% AA-G in 25 mM PBS (pH 6).

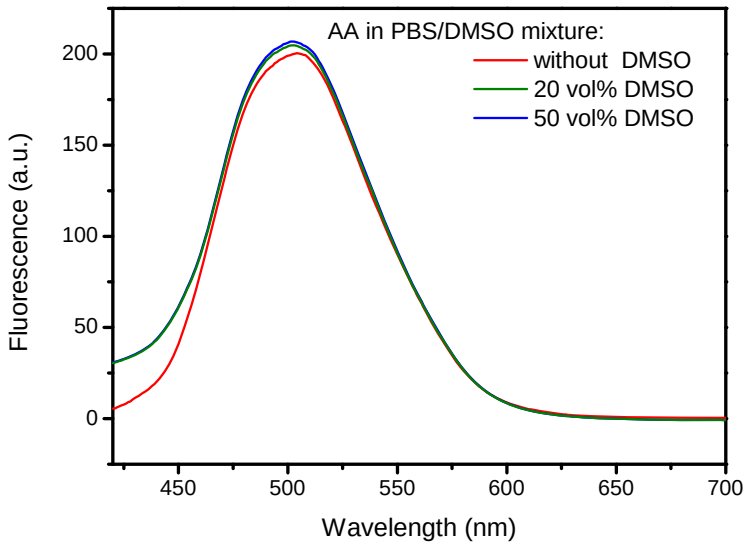

Fig. S7. Fluorescence spectra of 5 μg/mL AA in PBS/DMSO mixture containing 0, 20, and 50 vol% DMSO, respectively. Excitation=400 nm.

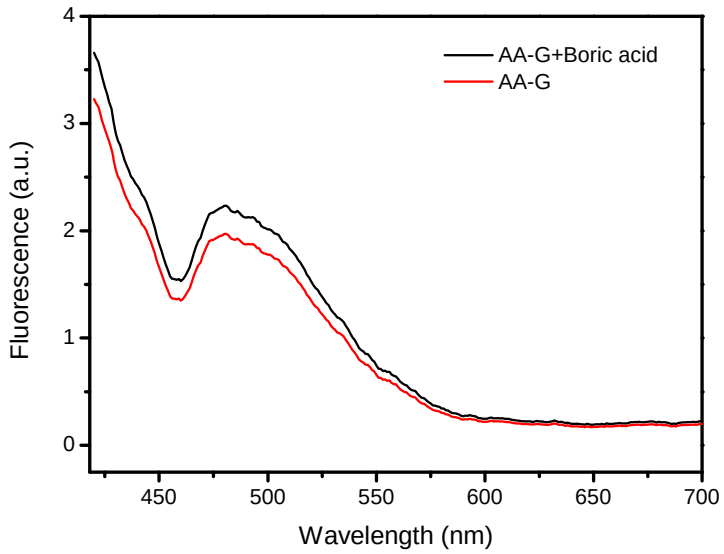

Fig. S8. Fluorescence spectra of AA-G in 25 mM PBS (pH 6) in the presence and absence of 100 mM boric acid. Excitation=400 nm.

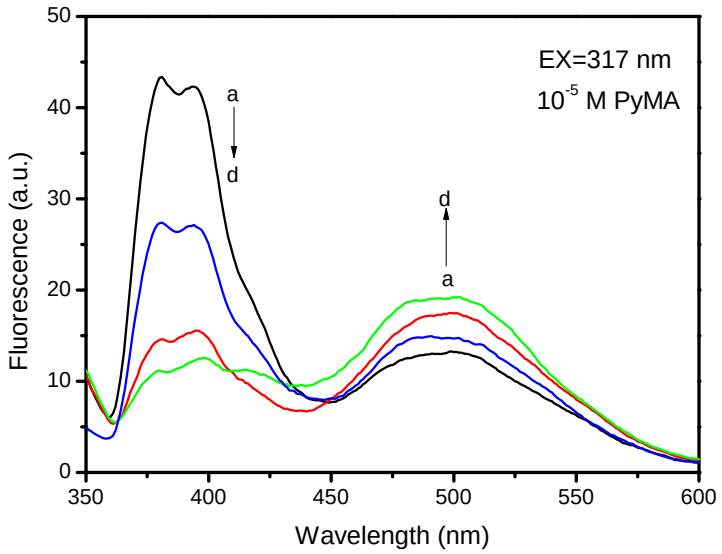

Fig. S9. Time-dependent fluorescence spectra of AA-G in 25 mM PBS (pH 6) upon adding 10^{-5} M PyMA. Curves a, b, c, and d were recorded at 1, 4, 7, 10 min after adding PyMA, respectively.

The structure of PyMA:

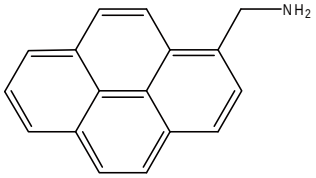

PyMA can be included inside the helical cavity of amylose. FRET between AA-G and PyMA takes place.

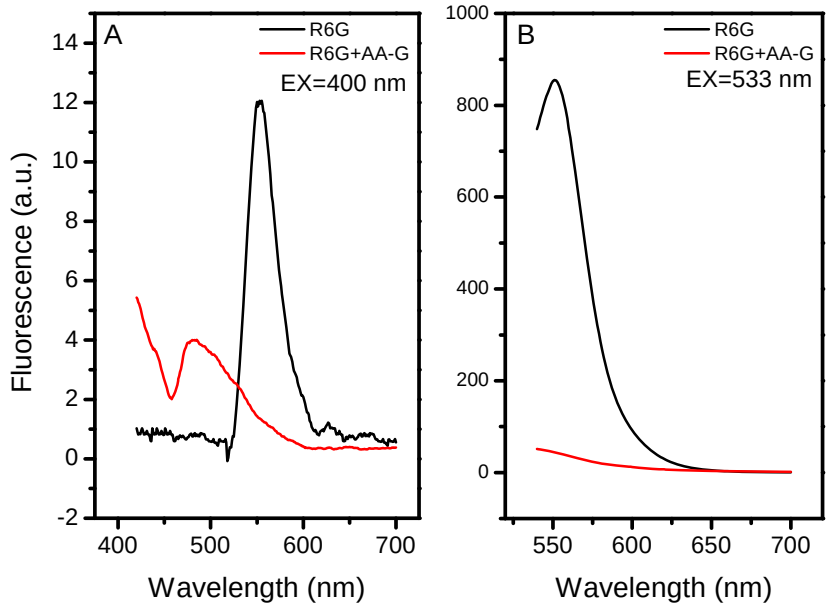

Fig. S10. Fluorescence spectra of AA-G in 25 mM PBS (pH 6) in the presence and absence of 10^{-5} M R6G with the excitation of (A) 400 nm and (B) 533 nm.

The structure of R6G:

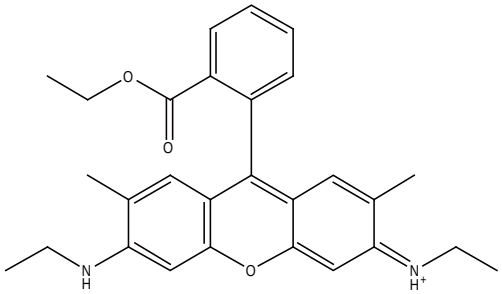

The structure and size of R6G determines that R6G CAN NOT be included inside the helical cavity of amylose. Therefore, no FRET between AA-G and PyMA takes place.

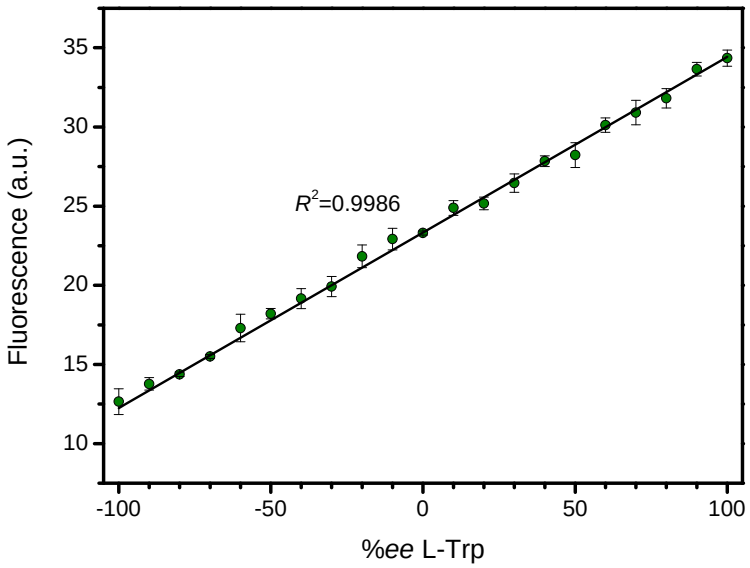

Fig. S11. Plot of fluorescence against %*ee* of L-Trp showing the linear dependence. The *ee* was defined as *ee*= ([L-Trp] - [D-Trp])/([L-Trp] + [D-Trp]), where [L-Trp] and [D-Trp] represent the concentration of L- and D-Trp, respectively. The total concentration of L- and D-Trp ([L-Trp] + [D-Trp]) was kept at 75 μM.